
Article:
Savić, N.D. orcid.org/0000-0002-6593-3499, Declerck, K. orcid.org/0000-0003-3711-7344, Prasad, R.R.R. orcid.org/0000-0002-8724-6358 et al. (3 more authors) (2025) Programmable 2D metal-organic framework nanosheets for enzyme-like hydrolysis of large proteins. Advanced Functional Materials, 35 (22). 2504117. ISSN 1616-301X

https://doi.org/10.1002/adfm.202504117

WILEY-VCH

Programmable two-dimensional metal-organic framework nanosheets for enzyme-like hydrolysis of large proteins

Nada D. Savić, Kilian Declerck, Ram R. R. Prasad, Givi Kalandia, Jonathan A. Foster, Tatjana N. Parac-Vogt**

N. D. Savić, K. Declerck, G. Kalandia, T. N. Parac-Vogt
Department of Chemistry
KU Leuven, 3001 Leuven, Belgium
E-mail: tatjana.vogt@kuleuven.be

Ram R. R. Prasad, Jonathan A. Foster
Department of Chemistry
The University of Sheffield,
Brook Hill, Sheffield S3 7HF, UK
E-mail: jona.foster@sheffield.ac.uk

Keywords: metal-organic framework nanosheets (MONs), zirconium; metalloproteases, protein hydrolysis, dipeptide hydrolysis

Abstract: The development of materials that mimic the catalytic activity of natural enzymes, so called nanozymes, are of crucial importance in biochemical and biotechnological fields. A new Zr-pyridine tribenzoate metal-organic framework nanosheet (MON), Zr-PTB with 6-connected Zr_6O_8 clusters was synthesized via a formic acid modulated solvothermal synthesis. The catalytic activity of MON, graphene-like two-dimensional materials which possess large external surface areas and tunable properties, is reported for the first time towards peptide bond hydrolysis of various peptides and proteins. Structure-reactivity analysis and the comparison with Zr-BTB (BTB = 1,3,5-tri(4-carboxyphenylbenzene)), a structural analogue of Zr-PTB with more hydrophobic linker, revealed a delicate interplay between coordination bonds and hydrophobic interactions with the MON's surface as the main driving forces influencing reactivity. Compared to 3D MOFs, Zr-PTB produced a larger number of peptide fragments, indicating the importance of larger external surface area with easily accessible catalytically active sites for more comprehensive hydrolysis of proteins. The advantage of 2D MONs with respect to 3D MOFs, where pore sizes and diffusion of large substrates is a limiting factor influencing their reactivity, is further reflected by the ability to hydrolyze very large proteins. The exceptional stability of Zr-PTB allowed for its recyclability for over 5 reaction cycles.

1. **Introduction**

The high inertness and remarkable stability of the peptide bond, with an estimated half-life for hydrolysis ranging from 350 - 600 years at 25 °C in aqueous solutions and at physiological pH, makes peptide bond cleavage a challenging task.[1] However, the cleavage of peptide bonds has found a vast variety of applications in different pharmaceutical and biotechnological fields, and most notably in the field of proteomics.[2–4] In general, peptide bonds can be cleaved either via oxidative, photooxidative, or hydrolytic mechanism.[1,5–7] Oxidative and photooxidative protein cleavage is mainly employed in redox proteomics studies, where protein modifications and alterations caused by various diseases are investigated.[8,9] However, these processes cause covalent modifications of the N- and C- terminal groups of the resulting fragments as well as of some side chain residues that complicate structural analysis. In contrast, hydrolytic cleavage produces peptides in which N- and C- terminal groups are in their native form and the proteins are cleaved into smaller and well-defined peptide fragments. As a result, hydrolytic cleavage is preferred in classical proteomics workflows, regardless of the employed approach (bottom-up or middle-down).[10,11] Currently, natural proteases are generally used for hydrolytic protein cleavage, with trypsin being the most commonly employed one.[12] However, natural proteases face many challenges such as a high cost, incompatibility with non-physiological reaction conditions, a tendency to form short peptide fragments that hamper coverage of the whole proteome and affinity towards self-digestion which contaminates the analyte and hinders further analysis.[4,12] Additionally, in the field of middle-down proteomics, there is an urgent need for the development of artificial proteases that are capable of producing peptide fragments within the size range of 3-10 kDa. These proteases would assist in improving the analysis of proteins by generating fragments of appropriate size for efficient structural analysis using advanced mass spectrometry techniques.

To overcome shortcomings of natural proteases, various metal complexes[1] and metal-oxo clusters (MOCs) such as metal substituted polyoxometalates [13–15] have been developed as artificial proteases. However, the reported reaction rates are rather slow, and the homogeneous nature of the catalyst requires additional and time-consuming steps to achieve its separation from the proteolytic mixture. More recently, different materials with biomimetic properties were explored,[16–19] among which metal-organic frameworks (MOFs) emerged as the most interesting alternatives to natural proteases due to their tunable features such as porosity, particle size, structural connectivity, ligand type, recyclability, stability, and reactivity.[14,20] Furthermore, their heterogeneous nature allows for efficient separation from the proteolytic mixture by simple centrifugation. In general, cluster-based MOFs are porous crystalline

organic-inorganic hybrid materials constructed of MOCs connected by various multitopic organic linkers, where the cluster core is responsible for the hydrolytic activity.[20] Catalytic activity towards peptide bonds has been established for a wide array of Zr- and Hf-MOF architectures ranging from the 6-connected Zr_6O_8 clusters in MOF-808 and MIP-201, to the 8- and 12-connected M_6O_8 (M = Zr(IV)/Hf(IV)) clusters in NU-1000 and UiO-66.[21–27] However, while some of these 3D materials showed high catalytic activity and stability in a wide range of different reactions conditions, their relatively small pore apertures restrict access of larger substrates to active sites embedded within the MOF structure. This ultimately results either in pore clogging or in reduced catalytic activity that is likely limited to the MOF's surface.

In this respect, MONs emerge as an attractive alternative due to their programmable and easily accessible two-dimensional (2D) structures. [28,29] MONs can be regarded as 2D analogues of MOFs and share some key features such as the diversity and tunability of their properties. Moreover, the structural anisotropy and nanoscopic dimensions of MONs increase their utility in various applications ranging from photo- and electro-catalysis, sensing, electronics, separation, and as photo functional nanomaterials.[29–31] In particular, Zr_6O_8 cluster-based MONs have been shown to outperform their three-dimensional (3D) counterparts in terms of reactivity due to the exceptionally high external surface area that permits facile access to the active sites of the larger substrates, in contrast to MOFs where the majority of active sites are buried within the microporous structure.[29,32–35] Furthermore, the readily dispersible nature makes them highly interesting to be developed as nanozymes.[36] Despite these advantages, MONs have been virtually unexplored as catalysts for biomolecular transformations.

Herein we report the synthesis of a new Zr_6O_8 cluster-based tricarboxylate MON, Zr-pyridine tribenzoate, (Zr-PTB), and explore its nanozymatic activity towards challenging peptide bond hydrolysis in various dipeptides and protein substrates. The design of the Zr-PTB MON was based on the incorporation of a linker that contains a pyridine moiety, which could facilitate interaction with the substrates via hydrogen bonding and promote reactivity by stabilizing intermediate reactions, similar to the natural proteases. As a comparison, an isoreticular structural analogue, Zr-BTB (BTB = 1,3,5-tri(4-carboxyphenylbenzene)), (**Figure 1**) which contains a benzene moiety instead of pyridine and therefore cannot engage in hydrogen bonding interactions, was synthesized and its hydrolytic activity toward peptides and proteins was also investigated to establish the influence of the linker's properties on substrate adsorption and hydrolysis efficiency of the MONs. The inferior performance observed in the reactions between Zr-BTB and different substrates additionally confirmed the validity of the

Zr-PTB synthesis and emphasizes the importance of the subtle changes in the ligand's functionality on the effectiveness of the MON's nanozymatic activity.

2. **Results and discussion**

2.1. **Synthesis and characterization**

Zr-PTB was synthesized using the H_3PTB linker (4,4',4''-(pyridine-2,4,6-triyl)tribenzoic acid),[37] via a formic acid modulated solvothermal synthesis that was optimized by modifying the procedure reported for the isoreticular Zr-BTB MON (**Figure 1(A)**).[38] The PXRD pattern of Zr-PTB showed good agreement to the PXRD pattern of Zr-BTB,[39] confirming its isoreticular structure (**Figure 1(B)**).

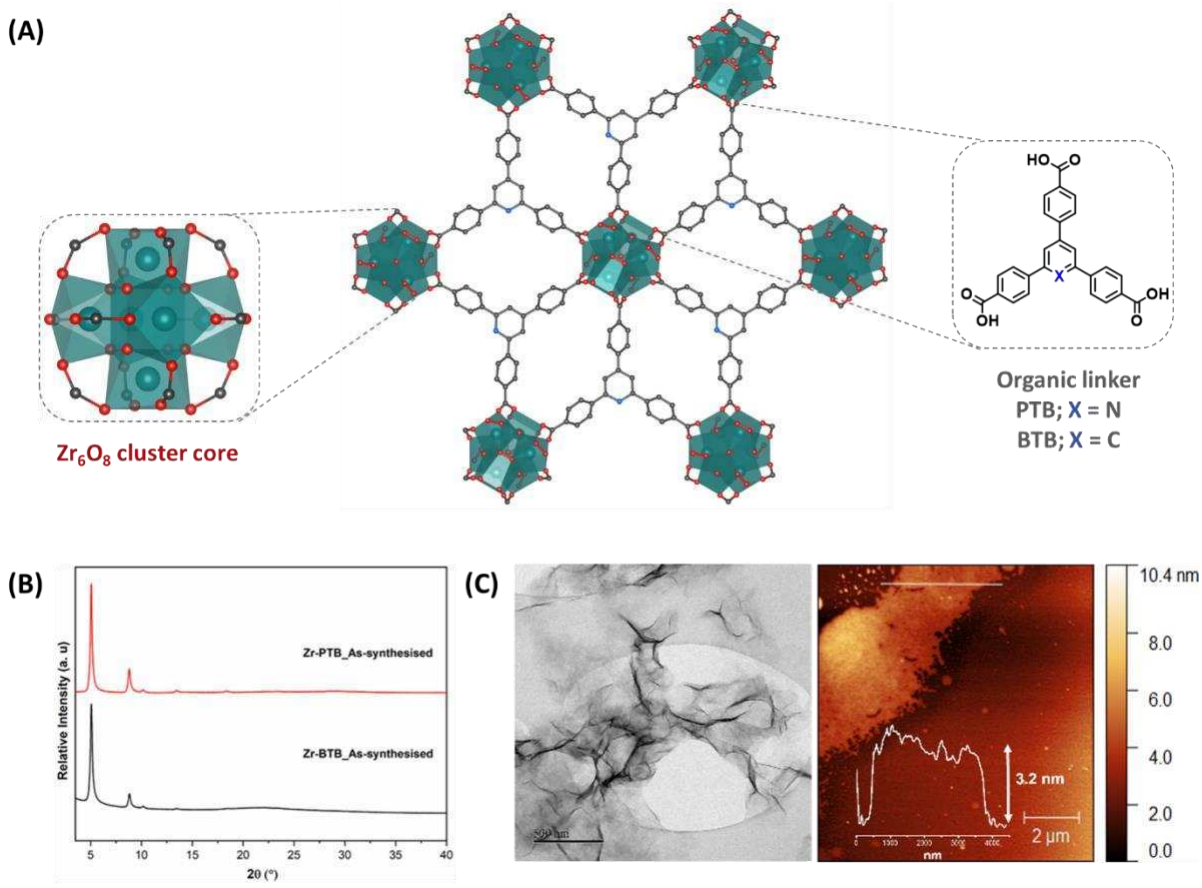

Figure 1. (A) Polyhedral and ball and stick representation of the 6-connected Zr_6O_8 cluster of Zr-PTB with capping formate ligands and PTB/BTB organic linkers (Color code: Zr, teal; O, red; C, black; N, blue. Hydrogen atoms are omitted for clarity); **(B)** The comparison of PXRD patterns of synthesized Zr-PTB with Zr-BTB;[39] **(C)** TEM and AFM images of Zr-PTB.

This data is consistent with the expected structure for Zr-BTB in which 6-connected Zr_6O_8 clusters are laterally connected by tritopic BTB linkers forming an infinite 3,6-connected network of Kagome topology. Solution-state ^{1}H NMR of the MON also showed peaks that correspond to the linker and cluster-coordinated formate (**Figure S1**). The capping formate groups enable anisotropic growth in two dimensions and give rise to Zr-PTB with the cluster formula $Zr_6(\mu_3\text{-}O)_4(\mu_3\text{-}OH)_4(HCOO)_6(PTB)_2$ (**Figure 1(A)**). Scanning electron microscopy (SEM) measurements (**Figure S2 (A)**) of Zr-PTB showed a wrinkled nanosheet morphology that was also supported by transmission electron microscopy (TEM) (**Figure 1(C)), Figure S2(B)**). Atomic force microscopy (AFM) images of Zr-PTB revealed high aspect ratio nanosheets with a bilayer thickness (**Figure 1(C), Figure S2(C)**), thus confirming the 2D nature of the material.

2.2. **Hydrolytic activity of Zr-PTB towards dipeptides**

2.2.1. Hydrolysis of glycylglycine (GG)

The hydrolytic activity of Zr-PTB towards peptide bonds was initially investigated using the simple dipeptide model system glycylglycine (GG) under various reaction conditions such as a different catalyst loading, substrate concentration, and pH. The formation of two equivalents of glycine (G) as the main reaction product, and the side product cyclic glycylglycine (cGG), which is formed through an intramolecular condensation of the carboxylate- and amino- terminal groups of GG, was monitored by ^{1}H NMR spectroscopy. Initially, the hydrolytic reactions were performed in D_2O in the presence of 2.0 mM of GG and 2.0 µmol of Zr-PTB (3.6 mg per 1 mL) at 60 °C and pD 7.0, similar to previous reports of MOF-catalyzed GG hydrolysis.[21–27] Before the reaction, the catalyst was dispersed by extended sonication (typically between 45 min and 1 h) providing fine separation of any aggregated MON nano-layers that could be caused by air drying. During the reaction, the signals between 3.82 – 3.84 ppm corresponding to GG decreased in intensity, whereas the intensity of the signal representing free G at 3.56 ppm increased (**Figure 2(A)**). The percentage of GG, G, and cGG were plotted as a function of time (**Figure 2(C))**, which showed that approximately 75.0 % of GG was converted to G after 24 h of incubation. Based on pseudo-first order reaction kinetics, the rate constant k_{obs} = 1.27 x 10^{-5} s^{-1} was calculated, which corresponds to a half-life ($t_{1/2}$) of 15.2 hours (**Figure 2(B)**). This represents a significant rate acceleration compared to the uncatalyzed reaction ($t_{1/2}$ = 6 years) under the same experimental conditions.[40]

The 6-connected Zr-PTB nanosheet showed faster reaction rates of GG hydrolysis than 8-connected NU-1000 and 12-connected UiO-66 MOFs ($t_{1/2}$ of 5 and 10 days, respectively) but very comparable rates to other 6-connected compounds such as MOF-808 and MIP-201 (**Table S1**).[21–24] Comparing the reactivity of Zr-PTB to previously reported Zr-MOFs is challenging, since Zr-MOFs reactivity is dependent on many different factors such as the cluster connectivity, particle size, missing linker defects, the structure of the linker etc.[14] However these results indicate that cluster connectivity is one the most important factor that dominates activity. For example, as it was mentioned, Zr-PTB shows similar reactivity as the 6-connected Zr_6O_8 cluster-based MOFs, even though the structural composition of the linker incorporated in the Zr-PTB is very different and more similar to the linker of NU-1000 (**Table S1**), suggesting that there is limited benefit of spatially positioning catalytically active Zr_6O_8 centers in the third dimension of MOF NU-1000. Although MOF NU-1000 has larger pores in comparison to MOF-808 and MIP-201, which could promote migration of the substrate to the catalytically active cluster cores in its microporous structure, the lower rate of hydrolysis implies that the presence of coordinatively unsaturated Zr(IV) centers, most likely on the surface of the MOFs, is key to determining the rate of observed reactivity.

Interestingly, when the catalytic performance of Zr-PTB was investigated without prior sonication, a lower rate constant was observed (k_{obs} = 7.42 x 10^{-6} s^{-1}), with a corresponding half-life ($t_{1/2)}$ of 26 hours (Figure S3). This indicates that sonication of the solid material increases its catalytic performance, presumably through the separation of MON nanolayers resulting in increased surface area. The increased accessibility of the catalytically active centers facilitates interaction of the substrate with the Lewis acidic Zr(IV) centers, which is essential for hydrolysis to occur.

The influence of the substrate concentration on the catalytic activity of Zr-PTB was investigated by incubating 2.0 μmol of Zr-PTB, which was sonicated prior to the reaction, and various amounts of GG (0.5 - 20 mM). The reactions were conducted at 60 °C and pD 7.0 (**Figure S4**). The activity of Zr-PTB was preserved even when a 5 times higher concentration of the substrate (10 mM) was used, where approximately 46.0 % of GG was converted to G after 24 h of incubation (**Figure S4**). To demonstrate the catalytic importance of Zr-PTB and rule out any contributions to hydrolysis from Zr(IV) ions that could leach in solution, Zr-PTB was removed from the reaction mixture and the supernatant was further incubated over 50 h at 60 °C. No further formation of G or cGG was observed, confirming the stability and high catalytic activity of the solid material (**Figure S5**).

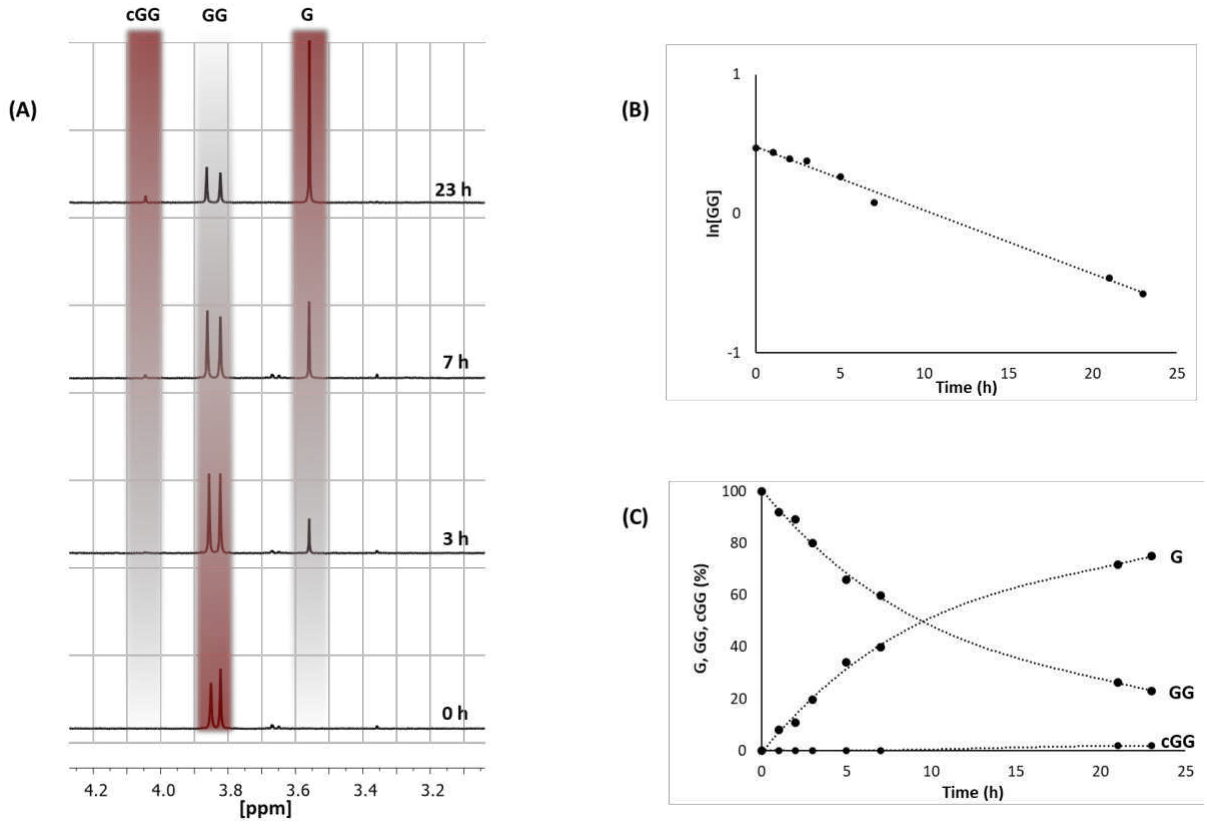

Figure 2. (A) Time dependent progress of the hydrolytic reaction of GG (2.0 mM) in the presence of Zr-PTB (2.0 µmol) at 60 °C and pD 7.0 followed by ^{1}H NMR spectroscopy; **(B)** Plot of ln[GG] as a function of time (h) showing first-order kinetics; **(C)** Percentage of GG, G, and cGG as a function of time.

The catalytic performance of Zr-PTB was further investigated in the pD range from 4.0 to 9.0, using the same reaction conditions as above (60 °C, 2.0 mM GG, and 2.0 µmol Zr-PTB) (**Figure S6-8**). At pD 4.0, a lower hydrolytic rate constant was observed (k_{obs} = 4.75 x 10^{-6} s^{-1}, $t_{1/2}$ = 40.5 h) **(Figure S6)**, while increasing the pD from 7.0 to 9.0 did not show significant improvement in the reactivity (k_{obs} = 1.19 x 10^{-5} s^{-1}, $t_{1/2}$ = 16.2 h) **(Figure S7)**. The Zr-PTB showed the highest reactivity around the pD 7.0 and 8.0 (**Figure S8**), which is a highly relevant range for biological systems and biochemical applications. The slight decrease in reactivity at pD 9.0 is most likely linked to the slight decomposition of Zr-PTB structure, as indicated by the presence of free PTB linker in solution (**Figure S7(A)**). The faster hydrolysis at neutral and mild alkaline conditions can be rationalized by the higher concentration of OD^-/OH^- nucleophile required for the hydrolysis of the peptide bond, as well as by favorable deprotonation of terminal carboxylic and amino functional groups of GG at higher pD values,[41] allowing for enhanced substrate-cluster interactions. Additionally, the higher pD values might promote the release of coordinated formate ligands and accelerate their exchange with incoming substrates,

leading to better catalytic performance. This was confirmed by downfield shifting and broadening of the peak that corresponds to the protons of the -CH_2 group in close proximity to the terminal amino group of GG, indicating interaction with Zr(IV) from the cluster node (**Figure S7(A)**).

Since adsorption of the substrate is an essential step that precedes the hydrolysis reaction, the adsorption of GG on the surface of Zr-PTB as a function of pD was followed by ^{1}H NMR spectroscopy (**Figure S9**). The spectra were recorded at different time intervals over 6 h at pD 4.0, 7.0, and 9.0 and at a temperature of 22 °C to prevent the hydrolysis reaction that could complicate interpretation of the results. At pD 4.0, adsorption of GG was less pronounced, which is in accordance with the lower reactivity observed at this pD value. This suggests the presence of electrostatic repulsion between the electrophilic Zr(IV) metal centers and the protonated amino group of GG (pKa = 8.16) (**Figure S9**).[41] Zeta potential measurements of Zr-PTB in water confirmed its positive charge (+38 mV), making electrostatic repulsion the most likely factor that inhibits effective interaction with the substrate. At pD 7.0, adsorption of GG increases, indicating a stronger interaction with the material due to lower electrostatic repulsion since the substrate is less positively charged. However, slightly lower adsorption was observed at pD 9.0, which is most likely due to reduced linker connectivity leading to missing linker defects that could lead to a decrease in hydrophobic and hydrogen bonding interactions with the substrate.[42] Therefore, bulky and hydrophobic PTB linkers incorporated into the MON's structure also influence its catalytic reactivity and interaction with substrate.

To test whether incorporation of a nitrogen atom within the organic linker of the new Zr-PTB structure influences the reactivity of the catalyst towards peptide bond hydrolysis, the isoreticular Zr-BTB nanosheet was probed as a catalyst for GG hydrolysis under the same conditions (pD 7.0, 60 °C). Interestingly, Zr-BTB showed much lower catalytic activity, with only 32.4 % of GG converted to G after 23 h (k_{obs} = 2.75 x 10^{-6} s^{-1}, $t_{1/2}$ = 70.0 h) (**Figure S10**), compared to the 75.0 % conversion observed in the presence of Zr-PTB. This drop in reactivity highlights the importance of subtle changes in the ligand structure on the reactivity of MONs and properties of MON surfaces. The presence of benzene instead of pyridine in the BTB ligand most likely prevents hydrogen bond interactions with the substrate which likely stabilize MON/substrate binding. Furthermore, the hydrophobicity of the surface of Zr-BTB is also larger in comparison to Zr-PTB, making product desorption more difficult. Therefore, the nature of the ligand should be carefully considered for the design of new MON catalysts for the hydrolysis of other peptide or protein substrates.

2.2.2. Reactivity of Zr-PTB towards Gly-X dipeptides

Since Zr-PTB showed superior reactivity compared to its analogue Zr-BTB, it was further used to evaluate the influence of the size, chemical nature and hydrophobicity of different amino acids on the peptide bond hydrolysis. Different Gly-X dipeptides (X = Ala, Asp, Thr, Glu, His, Lys, Phe, Met, Leu, Ile) (2.0 mM) were incubated with 2.0 µmol Zr-PTB at pD 7.0 and 60 °C for 7 h. The Hydrolysis rate of Gly-X peptide bond upon incubation with Zr-PTB was plotted as a function of the amino acid side chain volume and Rose hydrophobicity scale (**Figure 3**). In contrast to previously investigated Zr-MOFs, where the hydrolytic efficiency correlated well with the size of the dipeptides,[14] with smaller peptides showing the highest reactivity, such correlation was less obvious here. Instead, the highest reactivity of Zr-PTB was observed in the presence of dipeptides with hydrophobic side chain residues, in particular Gly-Phe, which contains a bulky benzene ring. This preference is most likely due to favorable interactions with the aromatic PTB linkers through π–π stacking and/or hydrophobic interactions (**Figure 3**). Despite the overall positive charge of Zr-PTB, indicated by its zeta potential, the reactivity towards dipeptides with negatively charged residues (Gly-Asp and Gly-Glu) was not significantly faster compared to other dipeptides. This most likely results either from the hydrophilic nature of these peptides or from the presence of additional carboxylic groups in the side chains of Asp and Glu residues that could coordinate to Zr(IV), thus preventing effective interaction with the carbonyl oxygen atom in the peptide bond, which is required for the hydrolytic reaction to occur.[43] The higher conversion of Gly-Asp in comparison to Gly-Glu is consistent with previous reports and can be ascribed to the formation of a more stable five-membered ring of the succinic anhydride intermediate for Gly-Asp in comparison to a less stable six-membered ring of the glutaric anhydride intermediate for Gly-Glu due to the shorter side chain of Gly-Asp connecting the two carboxylate groups.[14,44]

In contrast, the reactivity towards the positively charged dipeptide Gly-Lys was significantly slower, most probably due to electrostatic repulsion with Zr-PTB that could originate from the positively charged surface of the investigated MON. Although Gly-His might be also partially positively charged at pD 7.0, its reactivity with Zr-PTB was rather high. This could be due to its relatively high hydrophobicity that facilitates interactions with the PTB linker, or due to coordination of the nitrogen atom in the imidazole ring of His to the Zr(IV) clusters, bringing the peptide bond into close proximity to the catalytically active metal center and therefore accelerating hydrolysis.[15]

These results indicate that the main factors influencing the rate of peptide bond hydrolysis are the chemical nature and hydrophobicity of the amino acids in the dipeptide. Since the surface of the MONs can be changed by modifying the organic linkers that connect the hydrolytically active cluster cores, this opens possibilities for further tuning of the interactions with biomolecules and the catalytic performance of the MON as well.[32]

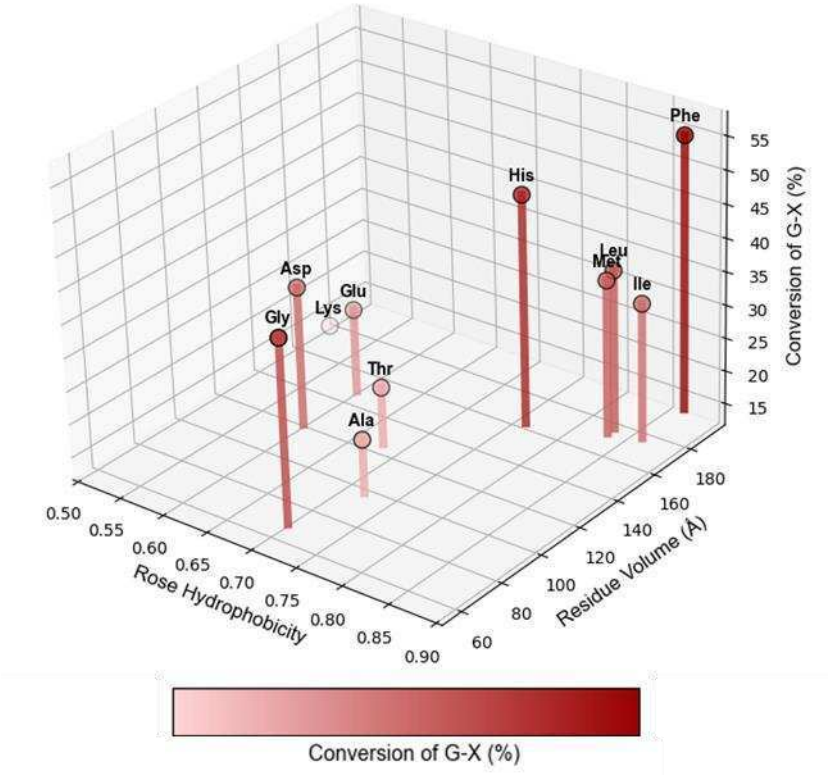

Figure 3. Conversion of Gly-X (2.0 mM) based on the loss of the dipeptides in solution after 7 h at 60 °C and pD 7.0 in the presence of Zr-PTB (2.0 µmol) as a function of the **(A)** volume of the amino acid side chain and **(B)** Rose hydrophobicity scale.[45]

2.2.4. Recyclability of the catalyst

The heterogeneous nature of Zr-PTB enabled easy recovery from the reaction mixture by simple centrifugation. The recyclability of Zr-PTB was confirmed by monitoring its reactivity towards GG over 5 reaction cycles. In order to remove potentially unreacted GG or any of the formed products, Zr-PTB was washed after each cycle with various organic solvents (ethanol, methanol, and acetonitrile) or water for 24 h at 22 °C. After air drying of Zr-PTB, a new reaction cycle was set up by addition of the same amount of substrate (2.0 mM) under identical reaction conditions and the reaction progress was followed by ^{1}H NMR spectroscopy, while Zr-PTB was sonicated prior to each separate reaction cycle. The catalytic performance of Zr-PTB was reduced when organic solvents were used in the washing process, with a

conversion of 42.0 - 48.3 % of GG after five reaction cycles (**Figure 4**). This most likely results from the lack of an activation step to remove Zr(IV)-coordinated solvents, which requires vacuum drying of the material at elevated temperatures. This step was omitted in order to avoid potentially stronger stacking of the nanosheets, but it might induce coordination of the solvents to the catalytically active centers of the cluster node, thereby reducing the availability of free coordination sites and further inhibiting interaction with GG and further hydrolysis.

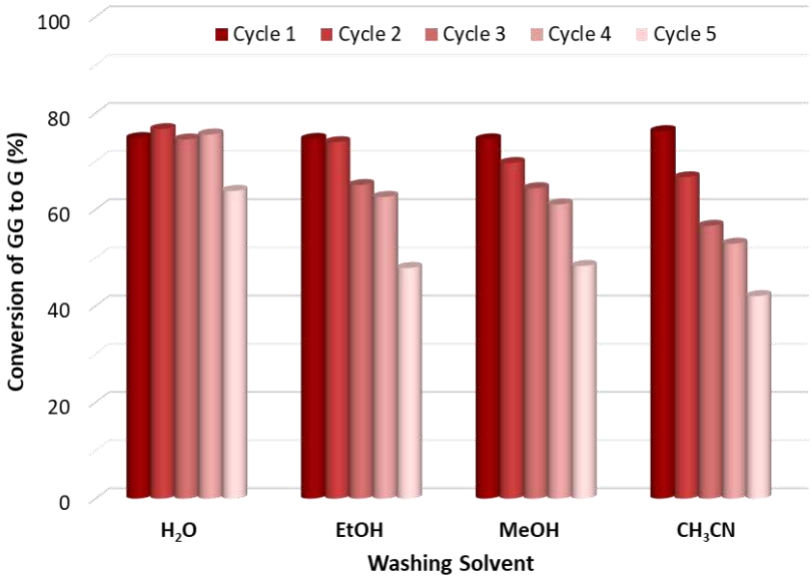

Figure 4. Conversion of GG (2.0 mM) to G in the presence of Zr-PTB (2.0 µmol) after 24 h at 60 °C and pD 7.0 over 5 reaction cycles following washing procedure with different solvents.

However, when performing the washing step in water, the catalytic activity of Zr-PTB was preserved over five reaction cycles, indicating the viability of a washing procedure (**Figure 4**). This is in contrast with the recyclability of some previously investigated 6-connected MOFs (MIP-201 and MOF-808) whose reactivity was significantly diminished when using water in the washing process, attributed to blocking of the MOF micropores preventing migration of the substrate. For example, MOF-808 showed a 90 % lower activity in the second cycle of the reaction, while the activity of MIP-201 decreased by approximately 20 %.[22,23] On the other hand, the catalytic activity of Zr-PTB remained identical after the second cycle and was reduced only by ca. 10 % after the fifth cycle of the reaction (**Figure 4**). The excellent recyclability of Zr-PTB increases its applicability, especially since the time-consuming and energy-intensive activation step that is usually conducted in MOF-catalyzed reactions can be avoided.

2.3. **Hydrolytic activity of Zr-PTB towards proteins**

The protease activity of Zr-PTB was investigated using two proteins with different molecular weight (Mw) but similar isoelectric point (pI), horse heart myoglobin (Mb) (16.9 KDa, 154 residues, pI 6.9) and hemoglobin from bovine blood (Hb) (64.7 KDa, 572 residues, pI 6.8). It was previously shown that both the nature and size of smaller substrates (dipeptides) influence the hydrolytic activity of Zr-PTB. Therefore, we aimed to investigate its catalytic activity toward two proteins that significantly differ in terms of size (the diameter of Mb is 3.5 nm while Hb has a diameter of 5.5 nm).[46] These properties might affect their interaction and adsorption at the surface of the Zr-PTB nanosheet, as well as its hydrolytic efficiency. While the reactivity of MOFs has been described in detail for smaller proteins, a comparison between the reactivity of MOFs toward differently sized proteins has never been performed.

Initially the hydrolysis of Mb (0.02 mM) by Zr-PTB (2.0 μmol) was evaluated in aqueous solution at 60 °C by taking aliquots at different time intervals (4 h, 10 h, and 48 h) and analyzing them by sodium dodecyl sulfate polyacrylamide gel electrophoresis (SDS-PAGE). During the hydrolysis reaction, severe adsorption of the native protein and formed proteolytic fragments occurred on the surface of Zr-PTB as observed from the low intensity of the bands in gel electropherogram. Therefore, an elution protocol was developed to recover the proteolytic fragments by incubating the centrifuged solid material with a 4.0 % NH_4OH solution for 72 h at 22 °C, prior to performing the SDS-PAGE analysis (**Figure 5**). This resulted in the appearance of 10 new fragments with an approximate molecular weight (Mw) of 15.4; 14.6; 12.9; 11.1; 10.5; 8.1; 7.6; 6.1; 4.6; and 3.6 kDa, which indicated that Mb was hydrolyzed in a controlled manner. It is worth highlighting that the obtained fragments are of an ideal size for analysis by the middle-down proteomics (3 – 15 kDa) approach, which is important as a limited number of natural proteases can produce fragments in this size range.[11] In comparison to several Zr_6O_8-based MOFs, Zr-PTB produced more fragments under the same reaction conditions. For example, MIP-201 yielded 6 fragments after 24 h and MOF-808 yielded only 4 fragments after 48 h.[23,47] This indicates that the larger external surface area of Zr-PTB with easily accessible catalytically active sites enables faster and more comprehensive hydrolysis of Mb.

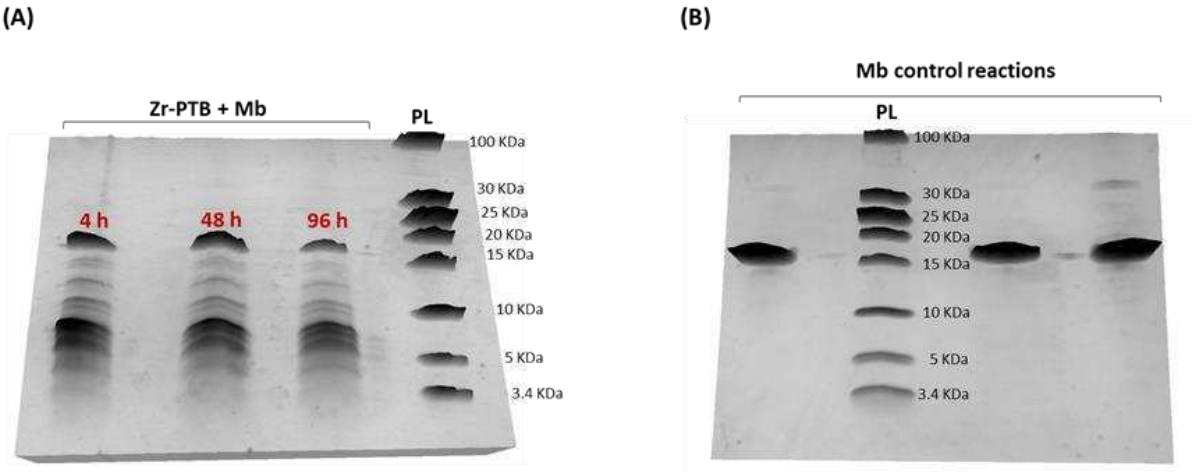

Figure 5. Coomassie stained SDS-PAGE gel of **(A)** Mb (0.02 mM) in the presence of Zr-PTB (2.0 µmol) after 4 h, 10 h, and 48 h at 60 °C in aqueous solution, eluted with 4.0 % NH_4OH for 72 h. PL - protein ladder; **(B)** Mb (0.02 mM) incubated at 60 °C in water for 96 h (first lane); in 4.0 % NH_4OH for 24 h at 22 °C (second lane) and in 4.0 % NH_4OH for 72 h at 22 °C (fourth lane). PL - protein ladder.

The hydrolytic reactions were further investigated in the presence of different amounts of Zr-PTB ranging from 0.2 to 2.0 µmol and at the same Mb concentration (0.02 mM) to explore the effect of catalyst loading on protein adsorption. Several elution protocols were performed using either water or 0.3 - 4.0 % NH_4OH solutions (**Figure S11, S12**). The reactions performed in the presence of a lower amount of catalyst (0.2, 0.5, or 0.7 µmol) required only 1.0 % NH_4OH for visualization of the fragments by SDS-PAGE. However, at a higher catalyst loading (1.0, 1.5, or 2.0 µmol), a harsher elution protocol consisting of 4 % NH_4OH was needed for the recovery of all generated fragments (**Figure S12**), indicating that protein adsorption is indeed influenced by the amount of Zr-PTB catalyst.

The alkaline medium resulting from the presence of NH_4OH may cause protein degradation by breaking the peptide bonds. Several control experiments were therefore conducted by incubating the protein in a 4.0 % NH_4OH solution (pH 11.0). No protein fragments were observed after 72 h of incubation in 4.0 % NH_4OH at 22 °C indicating the structure of Mb was preserved (**Figure 5(B)**).

In contrast to Zr-PTB, its isoreticular analogue Zr-BTB was much less effective as a nanozyme toward Mb hydrolysis. Hydrolytic reactions of Mb (0.02 mM) in the presence of Zr-BTB (2.0 µmol) at 60 °C were performed by taking aliquots at different time intervals (4 h, 10 h, and 48 h). However, the SDS-PAGE gel electropherogram showed that very weak hydrolytic

fragments were produced during the hydrolytic process, which were visualized by using the same elution protocol, 4.0 % NH_4OH solution for 72 h at 22 °C **(Figure S13**). Furthermore, the Zr-BTB powder remained red after elution, indicating that Mb was still strongly adsorbed. This is attributed to the presence of a benzene instead of pyridine in the center of the linker, resulting in a more hydrophobic surface compared to Zr-PTB. Stronger binding interactions could prevent structural reorganization of the protein, thus limiting favorable interaction with the catalytically active Zr(IV) cluster core. Furthermore, stronger adsorption may also cause inefficient fragment desorption, thus poisoning the Zr-BTB catalyst and lowering its reactivity.

In contrast to the previously investigated 3D MOFs,[14] their 2D analogues are composed of finely dispersed nanolayers with easily available catalytically active sites. In order to investigate the accessibility of catalytically active cluster units, as well as the reactivity of the material, the hydrolysis of the larger tetrameric protein Hb was investigated. The hydrolysis of Hb (0.02 mM) was carried out in the presence of 2.0 μmol Zr-PTB at 60 °C in aqueous solution. The formation of 8 new hydrolytic fragments with approximate Mw of 12.0; 10.7; 9.1; 7.5; 7.0; 5.9; 5.2; 4.0 kDa was demonstrated by SDS-PAGE after elution with 4.0 % NH_4OH that was required for the recovery of the peptide fragments (**Figure S14(A)**). The control experiments showed that elution conditions (4.0 % NH_4OH) did not cause hydrolysis of peptide bonds (**Figure S14(B)**). These results indicate that the proteins with larger sizes could be hydrolyzed in the presence of Zr-PTB, with Hb being the largest protein hydrolyzed by any Zr-based cluster material so far.

2.4. Stability of the catalyst

To prove the effectiveness of Zr-PTB, its stability was investigated under the experimental conditions (pH 4.0 - 9.0 at 60 °C) and in the presence and absence of the peptide and protein substrates (GG and Mb). Furthermore, the effect of 1.0 - 4.0 % NH_4OH on the structure of material, which was used as eluent for the recovery of the proteolytic fragments was also explored. Several complementary techniques were used for this purpose including powder X-ray diffraction (PXRD), Fourier-transform infrared spectroscopy (FT-IR), scanning electron microscopy (SEM), inductively coupled plasma optical emission spectroscopy (ICP-OES), and proton nuclear magnetic resonance spectroscopy (^{1}H NMR). PXRD data showed preserved crystallinity and excellent stability of Zr-PTB under all investigated reaction conditions (**Figure 6(A)**). Furthermore, the unchanged FT-IR spectra confirmed that the structural composition of Zr-PTB, and linker coordination in particular, was preserved (**Figure S15**). SEM measurements indicated that the morphology of Zr-PTB shows high resemblance

to its morphology after 24 h of incubation, even in the presence of GG and Mb (**Figure 6(B)**). This explains the outstanding recyclability of Zr-PTB, even after 5 reaction cycles. However, SEM measurements showed that incubation of Zr-PTB in the presence of 1.0 and 4.0 % NH_4OH solutions for 72 h at 22 °C significantly changed the texture of the solid material, even after extended rewashing and intensive activation in water (**Figure S16**). However, the PXRD patterns and IR spectra indicate that the crystallinity and chemical structure are still preserved (**Figure 6(A), S15**). Therefore, the changes in the MON's morphology are likely caused by changes in the overall surface charge, which could induce aggregation of individual nanolayers (**Figure S16**).

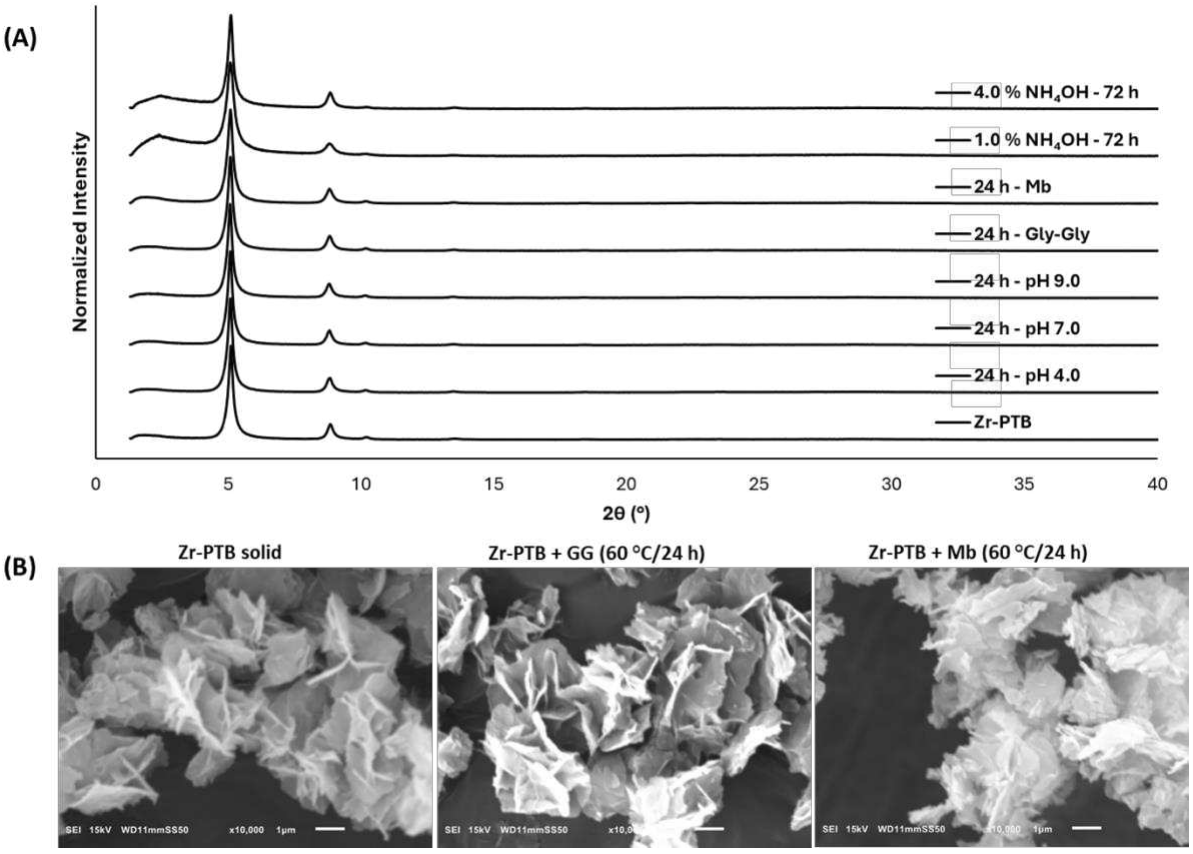

Figure 6. (A) PXRD patterns of Zr-PTB after incubation at 60 °C at different pH values, after the hydrolytic reaction in the presence of the GG or Mb and after incubation in the presence of 1.0 or 4.0 % NH_4OH at 22 °C; **(B)** SEM micrographs of Zr-PTB as synthesized and after 24 h of incubation in the presence of GG and Mb at 60 ºC.

ICP-OES measurements of the supernatant after incubation of Zr-PTB under various reaction conditions revealed that a negligible concentration of Zr(IV) ions leached into solution (< 60 ppb Zr(IV) were detected). This further proves that hydrolysis of dipeptides and proteins is caused by the solid Zr-PTB catalyst and not by soluble species resulting from degradation of the MON. Finally, ^1H NMR spectra of the MON incubated in 1.0 and 4.0 % NH_4OH for 72 h

showed that only a small amount of PTB linker leached from the Zr-PTB framework (**Figure S17**), further supporting the stability of the catalyst.

3. **Conclusion**

In this work programmable 2D Zr(IV)-based MONs were developed as a novel type of catalyst for the hydrolysis of larger protein substrates. A new MON synthesized in this work, Zr-PTB, exhibited similar or better activity compared to the previously investigated 3D Zr-MOFs,[22–25] emphasizing the advantage of the 2D nature of MON architectures where all catalytically active sites are exposed on the surface of the material and readily accessible for interaction with incoming substrate. Investigation of a range of dipeptides differing in terms of size, functional groups, and hydrophobicity revealed the interplay between coordination bonds and hydrophobic interactions with the MON's surface as the main driving forces that influenced reactivity. Zr-PTB was also very efficient for the selective hydrolysis of two differently sized proteins, producing a larger number of peptide fragments compared to previously investigated 3D MOF analogues. This suggests that the larger external surface area of Zr-PTB, enables faster and more comprehensive hydrolysis of proteins, that cannot readily diffuse through 3D MOF pores, with hemoglobin being the largest protein hydrolyzed by any Zr_6O_8-based material so far. The importance of surface properties on MONs nanozymatic activity was revealed by the lower reactivity of isoreticular Zr-BTB analogue, which was attributed to its more hydrophobic surface causing stronger adsorption of the protein leading to reduced catalytic activity. These findings indicate that the activity of MONs is determined by a delicate balance of hydrophobic, electrostatic, and hydrogen bond interactions with the protein surface, which should be sufficiently dynamic in nature to allow reorganization of the protein for the activation of the peptide bonds to occur at the Zr_6O_8 catalytic site. In addition, Zr-PTB showed outstanding reactivity and stability under various reaction conditions, including physiologically relevant pH as well as more extreme pH ranges (pH 4.0 - 11.0), providing new opportunities for the development of MONs as a novel class of artificial proteases. Additionally, the heterogeneous nature and the exceptional stability of Zr-PTB allows its recyclability for over 5 reaction cycles, which could have a beneficial effect on its implementation in proteomics workflows.

To the best of our knowledge, this is the first example of peptide bond hydrolysis catalyzed by a two-dimensional metal-organic nanosheet and, more generally, the first example of protein hydrolysis by a 2D catalyst. Even though the Zr-PTB has the same Zr_6O_8 active sites as its 3D MOF analogues, it offers larger accessibility of the catalytic sites, as well as

exceptional stability and recyclability which incentivizes further development of novel 2D architectures with different connectivity, ligand decoration, and surface properties. These variations in structural differences are particularly interesting and this is currently under investigation since even small changes to the multitopic linkers, such as the introduction of one nitrogen atom, could drastically alter hydrolytic activity.

4. **Experimental Section/Methods**

Materials

Formic acid (97 %) was obtained from Alfa Aesar. *N,N*-dimethylformamide (DMF), 4,4',4''-(pyridine-2,4,6-triyl)tribenzoic acid (H_3PTB), zirconium Chloride ($ZrCl_4$) (98 %), anhydrous methanol, methanol (99.8 %), anhydrous acetone, acetonitrile, ethanol (99.8 %), ammonium persulfate (APS), sodium thiosulfate (99 %), and tris(hydroxymethyl)aminoethane were obtained from Acros Organics. D_2O, DCl, NaOD, NaOH, dipeptides, 3-(trimethylsilyl) propionic-2,2,3,3-d_4 acid sodium salt (TMSP-d_4), horse heart myoglobin (Mb), hemoglobin from bovine blood (Hb), ethylene glycol (99 %), formaldehyde solution, glutaraldehyde solution, propan-2-ol, and hydrochloric acid were purchased from Sigma-Aldrich. Glycerol was bought from Invitrogen. *N,N,N',N'*-tetramethyl ethylenediamine (TEMED) was obtained from Carl Roth. Acrylamide 4K solution (40 %) Mix 29:1 and acrylamide solution (40 %) Mix 19:1 were purchased from PanReact Applichem. Acetic acid (99.7 %), Coomassie Brilliant Blue and PageRuler Low Range Unstained protein ladder were bought from Thermo Fisher Scientific. Bromophenol blue was bought from Fluka Analytics. Tricine was procured from FluoroChem. Trichloroacetic acid was bought from VWR Chemicals. Dithiothreitol (DTT), silver nitrate, and sodium carbonate were bought from ChemLab. All chemicals were purchased as pure reagent grades and used without further purification.

Synthesis

Linker Synthesis: 4,4',4''-(pyridine-2,4,6-triyl)tribenzoic acid (H_3PTB) was synthesized according to our previously published procedure.[37]

Synthesis of Zr-PTB: Zr-PTB was synthesized according to the modified procedure[38] by addition of $ZrCl_4$ (0.108 mmol; 25.40 mg) and PTB (0.0725 mmol; 31.86 mg) to a 20 mL screw-cap glass vial. After addition of 12.5 mL DMF, the mixture was ultrasonically dissolved to obtain a clear solution. To the resulting solution, 2.5 mL formic acid and 0.7 mL H_2O were

added and stirred for a few seconds. The vial was then placed in a preheated oven at 120 °C and heated for 48 h. After completion of the reaction, the vial was taken out of the oven and cooled down to room temperature naturally. The obtained white colloidal suspension of Zr-PTB was centrifuged and washed multiple times with DMF, followed by methanol after which the sample was vacuum dried at 22 °C.

Synthesis of Zr-BTB: Zr-BTB was synthesized according to a previously published procedure.[39]

Methods for materials characterization

Powder X-ray diffraction (PXRD): The identity and phase purity of all the samples was determined by Powder X-ray diffraction (PXRD) using a Bruker-AXS D8 diffractometer with primary monochromation (Cu Kα1, λ = 1.5418 Å) and a LynxEye position sensitive detector in Bragg Brentano parafocussing geometry using either 0.5 - or 0.7 - mm quartz glass capillaries. PXRD patterns were measured over the 2Θ range of 3 - 50° for 1 h 30 min unless mentioned otherwise.

Nuclear Magnetic Resonance (NMR): Nuclear Magnetic Resonance (NMR) spectra were recorded on a Bruker Avance III HD 400 spectrometer equipped with a standard geometry 5 mm BBFO probe with a single z-gradient at 400 MHz NMR samples were prepared by adapting the method developed by *Taddei and co-workers*.[48] Around 10 - 15 mg of metal-organic materials were dissolved in 1 mL of 1 M NaOD in D_2O by vigorous stirring for 24 h and filtered through a cotton wool to remove solid particles.

Scanning electron microscopy (SEM): Scanning electron micrographs of Zr-PTB were obtained using TESCAN VEGA3 LMU SEM. All samples were sputter coated with gold in a TESCAN VEGA3 LMU SEM, functioning at 15 keV.

Atomic force microscopy: Atomic force micrographs were collected on a Bruker Multimode 5 Atomic Force Microscope (AFM), fitted with a Nokia 10x visualizing lens operating in soft-tapping mode in air. Bruker OTESPA-R3 cantilever with 20.4 mV drive amplitude and 290 kHz nominal resonance frequency were used. AFM samples were prepared by carefully adding 10 μL of MON suspension onto a freshly cleaved mica substrate surface heated at 10 °C above the boiling point of the solvent used.

Zeta Potential: The zeta potential (ζ) of solutions of Zr-PTB suspended in water at 25 °C was determined by measuring the backscattering at 173° of a 632.8 nm laser using a Zetasizer Nano ZSP (Malvern Panalytical Ltd., Malvern, UK). The measurement was performed using folded

capillary cells. The zeta potential of the particles in solution was determined by electrophoresis and laser Doppler velocimetry according to the Smoluchowski model, using the equipment software provided by the manufacturer (Zetasizer Software 7.12, Malvern Panalytical Ltd., Malvern, UK).

Peptide bond hydrolysis studies

The hydrolysis was performed at different pD values 4.0, 7.0, 9.0 and 60 °C in D_2O. Zr-PTB (3.6 mg; 2.0 µmol) was added to 990 µL of D_2O. Before the addition of the investigated dipeptides, the suspension was sonicated at 35 kHz in a 320 W sonicator bath for approximately 1 h at 22 °C to obtained finely dispersed MON layers. The dipeptides 2.0 mM (10 µL of 200 mM stock solution) were added to the suspension of sonicated Zr-PTB. The reaction mixture was adjusted to investigated pD with NaOD and DCl and incubated at 60 °C. After different time increments, Zr-PTB was removed from the reaction mixture by centrifugation at 14000 rpm for 30 min. TMSP-d_4 was added as internal standard to 500 µL of supernatant before recording the ^{1}H NMR spectra. The effect of different concentrations of GG ranging from 0.5 - 20 mM was investigated in the same way. The observed reaction rate constants were obtained by fitting peptide concentrations to a first order decay function.

Adsorption study

The adsorption was performed at pD 4.0, 7.0 and 9.0 at 22 °C. 990 µL of D_2O was added to Zr-PTB (3.6 mg, 2.0 µmol) and suspension was sonicated for approximately 1 h. Further, 10 µL of 200 mM GG was added to the previously activated Zr-PTB. The mixtures were adjusted to different pD values with NaOD or DCl. After a certain time interval, the mixtures were centrifuged by removing the solid material. The adsorption of GG was followed by ^{1}H NMR spectroscopy.

Recycling experiments

The recyclability of Zr-PTB for GG hydrolysis was tested over five reaction cycles. After each reaction cycle (hydrolysis reactions at pD 7.0 and 60 °C), the MON was separated through centrifugation and washed 3 times with water for 1 h to remove unreacted substrate and potentially adsorbed reaction products formed during hydrolysis. Further, after removing water by centrifugation, Zr-PTB was stirred in different solvents (water, ethanol, methanol, or acetonitrile) for 24 h. Zr-PTB was subsequently air dried, and the catalytic process was repeated as described above.

Protein Hydrolysis

The hydrolysis of Mb and Hb (0.02 mM) in the presence of different concentrations of Zr-PTB (0.2 - 2.0 μmol) and Zr-BTB (2.0 μmol) was performed in water. Samples were incubated at 60 °C and aliquots were taken at different time intervals. The hydrolytic reactions were analyzed by SDS-PAGE. Gels consisting of a stacking gel (4 % (w/v) polyacrylamide gel in 0.5 M Tris−HCl buffer pH 6.8) and a resolving gel (16 % (w/v) polyacrylamide in 1.5 M Tris−HCl buffer pH 8.8 gel) were prepared. Samples (15 or 30 μL) were mixed with sample buffer (5 or 10 μL) and heated at 95 °C for 5 min. The resulting solution (10 or 30 μL) was loaded onto the gel. Unstained Page Rulers was used as a molecular mass reference. Experiments were performed at 200 V for 1.5 h, using an Omni Page electrophoretic cell combined with an EV243 power supply. The visualization of formed peptide fragments in SDS-PAGE gels was accomplished with silver staining and colloidal Coomassie protocols. The images were taken using a Gel DocEZ Imager (Bio-Rad, Hercules, CA).

Stability measurements

Solution-state ^{1}H NMR spectra were recorded on a Bruker Avance 400 and 600 spectrometers, where TMSP-d_4 was used as an internal reference. PXRD patterns were collected on the Malvern PANalytical Empyrean diffractometer (in transmission mode) over a 1.3 – 45° 2θ range, using a PIXcel3D solid-state hybrid pixel detector and Cu anode (Cu Kα1: 1.5406Å; Cu Kα2: 1.5444Å). Fourier transform infrared spectra (FTIR) were recorded on a Bruker Vertex 70 ATR-FTIR spectrometer equipped with a 1064 nm laser source. Scanning electron microscopy (SEM) micrographs were recorded at 15 kV using a JEOL-6010LV SEM after depositing a palladium/gold layer on the samples with a JEOL JFC-1300 autofine coater under Ar plasma. Inductively Coupled Plasma-Optical Emission Spectroscopy (ICP-OES) was performed on a Perkin Elmer optical emission spectroscopy Avio 500 instrument. A calibration curve was prepared with a series of standard zirconium solutions in the concentration range of 0.001 – 50 ppm.

Supporting Information

Supporting Information is available from the Wiley Online Library.

Acknowledgements

N. D. S., K. D. and R. R. R. P. contributed equally to this work. T.N.P.-V. and K. D. thank KU Leuven for funding. N.D.S. (1267623N) acknowledges Research Foundation Flanders (FWO) for financial support and a senior post-doctoral fellowship. This research was further supported

by FWO through infrastructure grant I002720N. R. R. R. P and J. A. F thank EPSRC (EP/S021124/1) for funding. G. K. thanks FWO for a doctoral fellowship (1185522N).

References

[1] N. E. Wezynfeld, T. Frączyk, W. Bal, *Coord Chem Rev* **2016**, *327–328*, 166.

[2] B. Meyer, D. G. Papasotiriou, M. Karas, *Amino Acids* **2011**, *41*, 291.

[3] H. Molina, D. M. Horn, N. Tang, S. Mathivanan, A. Pandey, *Proc Natl Acad Sci U S A* **2007**, *104*, 2199.

[4] D. L. Swaney, C. D. Wenger, J. J. Coon, *J Proteome Res* **2010**, *9*, 1323.

[5] C. V. Kumar, A. Buranaprapuk, *Angew Chem* **1997**, *36*, 2085.

[6] I. E. Platis, M. R. Ermacora, R. O. Fox, *Biochem* **1993**, *32*, 12761.

[7] M. J. Davies, R. J. W. Truscott, *J Photochem Photobiol B* **2001**, *63*, 114.

[8] D. I. Pattison, A. S. Rahmanto, M. J. Davies, *Photochem Photobiol Sci,* **2012***,11,* 38.

[9] A. Mannaa, F. G. Hanisch, *J Proteome Res* **2020**, *19*,1.

[10] Y. Zhang, B. R. Fonslow, B. Shan, M.-C. Baek, J. R. Yates, *Chem Rev* **2013**, *113*, 2343.

[11] A. Cristobal, F. Marino, H. Post, H. W. P. Van Den Toorn, S. Mohammed, A. J. R. Heck, *Anal Chem* **2017**, *89*, 3318.

[12] L. Tsiatsiani, A. J. R. Heck, *FEBS J* **2015**, *282*, 2612.

[13] D. E. Salazar Marcano, N. D. Savić, S. A. M. Abdelhameed, F. de Azambuja, T. N. Parac-Vogt, *JACS Au* **2023**, *3*, 978.

[14] D. E. Salazar Marcano, N. D. Savić, K. Declerck, S. A. M. Abdelhameed, T. N. Parac-Vogt, *Chem Soc Rev* **2024**, *53*, 84.

[15] F. De Azambuja, J. Moons, T. N. Parac-Vogt, *Acc Chem Res* **2021**, *54*, 1673.

[16] J. Xu, N. Ji, M. Guo, Y. Wang, X. Xu, *Angew Chem* **2023**, *62*, e202304554.

[17] D. Chen, G. Xiao, J. Tang, L. zhao, S. Li, L. Li, B. Li, T. Lei, J. Wang, *Catal Letters* **2024**, *154*, 5757.

[18] A. M. Embaby, L. P. W. M. Lelieveldt, F. Diness, M. Meldal, *Chem Eur J* **2018**, *24*, 17424.

[19] N. Ji, J. Xu, Y. Wang, M. Guo, X. Xu, *Mater Today Chem* **2023**, *34,* 101823.

[20] C. Simms, A. Mullaliu, S. Swinnen, F. de Azambuja, T. N. Parac-Vogt, *Mol Syst Des Eng* **2023**, *8*, 270.

[21] H. G. T. Ly, G. Fu, F. de Azambuja, D. De Vos, T. N. Parac-Vogt, *ACS Appl Nano Mater* **2020**, *3*, 8931.

[22] H. G. T. Ly, G. Fu, A. Kondinski, B. Bueken, D. De Vos, T. N. Parac-Vogt, *J Am Chem Soc* **2018**, *140*, 6325.

[23] S. Wang, H. G. T. Ly, M. Wahiduzzaman, C. Simms, I. Dovgaliuk, A. Tissot, G. Maurin, T. N. Parac-Vogt, C. Serre, *Nat Commun* **2022**, *13*, 1284.

[24] A. Loosen, F. de Azambuja, S. Smolders, J. Moons, C. Simms, D. De Vos, T. N. Parac-Vogt, *Chem Sci* **2020**, *11*, 6662.

[25] S. Dai, C. Simms, I. Dovgaliuk, G. Patriarche, A. Tissot, T. N. Parac-Vogt, C. Serre, *Chem Mat* **2021**, *33*, 7057.

[26] A. Loosen, C. Simms, S. Smolders, D. E. De Vos, T. N. Parac-Vogt, *ACS Appl Nano Mater* **2021**, *4*, 5748.

[27] J. Moons, A. Loosen, C. Simms, F. de Azambuja, T. N. Parac-Vogt, *Nanoscale* **2021**, *13*, 12298.

[28] L. Cao, T. Wang, C. Wang, *Chin J Chem* **2018**, *36*, 754.

[29] J. Nicks, K. Sasitharan, R. R. R. Prasad, D. J. Ashworth, J. A. Foster, *Adv Funct Mater* **2021**, *31*, 2103723.

[30] D. J. Ashworth, J. A. Foster, *J Mater Chem A,* **2018***,6,* 16292-16307.

[31] A. C. Wood, E. C. Johnson, R. R. R. Prasad, M. V. Sullivan, N. W. Turner, S. P. Armes, S. S. Staniland, J. A. Foster, *Small* **2024**, 2406339.

[32] X. Feng, Y. Song, W. Lin, *J Am Chem Soc* **2021**, *143*, 8184.

[33] Y. Quan, G. Lan, Y. Fan, W. Shi, E. You, W. Lin, *J Am Chem Soc* **2020**, *142*, 1746.

[34] Z. Lin, N. C. Thacker, T. Sawano, T. Drake, P. Ji, G. Lan, L. Cao, S. Liu, C. Wang, W. Lin, *Chem Sci* **2018**, *9*, 143.

[35] W. Shi, Y. Quan, G. Lan, K. Ni, Y. Song, X. Jiang, C. Wang, W. Lin, *J Am Chem Soc* **2021**, *143*, 16718.

[36] L. Cao, C. Wang, *ACS Cent Sci* **2020**, *6*, 2149.

[37] R. R. R. Prasad, C. Pleass, A. L. Rigg, D. B. Cordes, M. M. Lozinska, V. M. Georgieva, F. Hoffmann, A. M. Z. Slawin, P. A. Wright, *Cryst Eng Comm* **2021**, *23*, 804.

[38] L. Cao, Z. Lin, F. Peng, W. Wang, R. Huang, C. Wang, J. Yan, J. Liang, Z. Zhang, T. Zhang, L. Long, J. Sun, W. Lin, *Angew Chem* **2016**, *128*, 5046.

[39] Z. Hu, E. M. Mahdi, Y. Peng, Y. Qian, B. Zhang, N. Yan, D. Yuan, J. C. Tan, D. Zhao, *J Mater Chem A Mater* **2017**, *5*, 8954.

[40] A. Radzicka, R. Wolfenden, *J Am Chem Soc* **1996**, *118*, 6105.

[41] A. Doğan, A. D. Özel, E. Kiliç, *Amino Acids* **2009**, *36*, 373.

[42] D. Yang, M. A. Ortuño, V. Bernales, C. J. Cramer, L. Gagliardi, B. C. Gates, *J Am Chem Soc* **2018**, *140*, 3751.

[43] S. Vanhaecht, G. Absillis, T. N. Parac-Vogt, *Dalton Trans* **2013**, *42*, 15437.

[44] H. G. T. Ly, T. T. Mihaylov, P. Proost, K. Pierloot, J. N. Harvey, T. N. Parac-Vogt, *Chem Eur J* **2019**, *25*, 14370.

[45] G. D. Rose, A. R. Geselowitz, G. J. Lesser, R. H. Lee, M. H. Zehfus, *Science* **1985***, 229,* 834.

[46] S. Papadopoulos, K. D. Jürgens, G. Gros, *Biophys J* **2000**, *79*, 2084.

[47] C. Simms, N. D. Savić, K. De Winter, T. N. Parac-Vogt, *Eur J Inorg Chem* **2022**, *2022,* e202200145.

[48] M. Taddei, R. J. Wakeham, A. Koutsianos, E. Andreoli, A. R. Barron, *Angew Chem* **2018**, *57*, 11706.

Nada D. Savić, Kilian Declerck, Ram R. R. Prasad, Givi Kalandia, Jonathan A. Foster, Tatjana N. Parac-Vogt**

Programmable two-dimensional metal-organic framework nanosheets for enzyme-like hydrolysis of large proteins

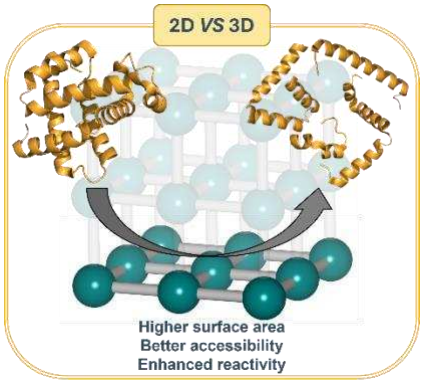

Metal-organic framework nanosheets (MONs) with different linker connectivity and exceptional stability are developed as a new class of heterogeneous nanozymes for peptide bond hydrolysis. Their larger surface area and heterogeneous nature provide superior active site accessibility and enhanced catalytic reactivity toward a wide range of dipeptides and proteins.